Trend Analysis and Forecast of Precipitation, Reference Evapotranspiration, and Rainfall Deficit in the Blackland Prairie of Eastern Mississippi

GARY FENG,[a] STACY COBB,[b] ZAID ABDO,[c,f] DANIEL K. FISHER,[d] YING OUYANG,[e] ARDESHIR ADELI,[a] AND JOHNIE N. JENKINS[a]

[a] *U.S. Department of Agriculture Agricultural Research Service, Mississippi State, Mississippi*
[b] *University of Georgia, Athens, Georgia*
[c] *U.S. Department of Agriculture Agricultural Research Service, Athens, Georgia*
[d] *U.S. Department of Agriculture Agricultural Research Service, Stoneville, Mississippi*
[e] *U.S. Department of Agriculture Forest Service, Mississippi State, Mississippi*

(Manuscript received 19 September 2015, in final form 25 March 2016)

ABSTRACT

Trend analysis and estimation of monthly and annual precipitation, reference evapotranspiration ET_o, and rainfall deficit are essential for water-resources management and cropping-system design. Rainfall, ET_o, and water-deficit patterns and trends at Macon in eastern Mississippi for a 120-yr period (1894–2014) were analyzed for annual, seasonal, and monthly periods. The analysis showed historical average annual rainfall, ET_o, and dryness index (DI) in the location to be 1307 mm, 1210 mm, and 0.97, respectively. Monthly rainfall and ET_o ranged from 72 to 118 mm and from 94 to 146 mm, respectively, between May and October, resulting in a monthly rain deficit from 22 to 62 mm. Annual rainfall showed an increasing trend of 1.17 mm yr^{-1} while annual ET_o exhibited a decreasing trend of −0.51 mm yr^{-1}, resulting in an annual DI reduction of 0.001 per year. Seasonal trends were found for rainfall in autumn (1.06 mm yr^{-1}), ET_o in summer (−0.29 mm yr^{-1}) and autumn (−0.18 mm yr^{-1}), and DI in autumn (−0.006). An autoregressive, integrated, and moving-average (ARIMA) approach was used to model monthly and annual rainfall, ET_o, and DI and to predict those values in the future. Low values of the root-mean-square error (RMSE) and mean absolute error (with both statistics being normalized to the mean of the observed values), low values of average percent bias, and low values of the ratio of the RMSE to the standard deviation of observed data, along with values of 1.0 for Nash–Sutcliffe modeling efficiency and the index of agreement, all suggest that the performance of the models is acceptable. The ARIMA models forecast 1319 mm of mean annual rainfall, 1203 mm of mean annual ET_o, and 0.82 of mean annual DI from 2015 to 2024. The results obtained from this research can guide development of water-management practices and cropping systems in the area that rely on this weather station. The approaches used and the models fitted in this study can serve as a demonstration of how a time series trend can be analyzed and a model fitted at other locations.

1. Introduction

Temperature, solar radiation, wind, rainfall, and reference evapotranspiration ET_o are the major climatic factors affecting agricultural production. Rainfall and ET_o are the most important variables for agricultural water management and hydrological processes. Seasonal changes in rainfall pattern may alter the hydrological cycle and environmental processes (Delitala et al. 2000) as well as the vegetation and the entire ecosystem (Lázaro et al. 2001). Rainfall is also the most sensitive component of watershed and agroecosystem models and affects all other components, which in turn affects the models' predictions of hydrological processes, water quality, and water quantity.

A good characterization of rainfall and ET_o trends and variability in time is necessary for many studies in climatology, hydrology, and agriculture. Analysis of the long-term trends in both precipitation and ET_o is essential for rain-fed farmland, which depends on rainfall conditions, and irrigated farmland, for which rainfall and ET_o greatly affect irrigation scheduling. The

Denotes Open Access content.

[f] Current affiliation: Colorado State University, Fort Collins, Colorado.

Corresponding author address: Gary Feng, Sustainable Agriculture Research Unit, USDA-ARS, 810 Highway 12 East, Mississippi State, MS 39762.
E-mail: gary.feng@ars.usda.gov

DOI: 10.1175/JAMC-D-15-0265.1

knowledge of trends in ET_o, rainfall, water deficit, and number of rainy days at different time intervals is very important for agricultural water use, regulation, and planning in any region. Accurately predicting trends of precipitation, ET_o, and water deficit can play an important role in irrigation scheduling, water-resources distribution planning and optimization, soil and water conservation, and cropping-system design.

Attention has been paid to analyzing time series trends of precipitation, ET_o, and water deficit because of public concern over climate change. Many studies have been conducted to address spatial patterns and temporal trends on global and regional scales. Increasing trends in air temperature and decreasing trends in ET_o have been detected in the past 50 years in North America (Burn and Hesch 2007; Hobbins et al. 2004). Both decreasing and increasing trends in mean annual rainfall have been reported (Roderick et al. 2009a,b). Precipitation has high spatial variability (Dyer and Mercer 2013), and therefore it is essential to conduct a detailed assessment of local temporal characteristics, patterns, and trends in rainfall, ET_o, and water deficit. Long-term time series analysis of past trends at local scales could lead to development of reliable prediction tools for forecasting ET_o, rainfall, and water deficit, which could provide for more efficient use of available water resources. The overall performance of statistical weather-forecasting methods and dynamic downscaling approaches of process-based climate models was similar for prediction of temperature and rainfall (Ahmed et al. 2013).

Mississippi is one of the most productive states in the midsouthern United States as a result of fertile soils, a relatively long growing season, and abundant annual rainfall. Unequal rainfall distribution throughout the year, as well as uncertain and unreliable rainfall during the growing season, has led to intensive irrigation in the region. In the western delta of Mississippi, over 90% of irrigation water is pumped from 18 000 water wells. Increasing groundwater withdrawal from the Mississippi River Valley alluvial aquifer has resulted in an alarming decline in aquifer levels. In the east-central Blackland Prairie of Mississippi, over 90% of irrigation water is pumped from ponds harvested from rainfall and runoff because groundwater is too deep and expensive to pump. It is critical, therefore, to better understand temporal trends, patterns, and variability in temperature and rainfall from past records and to try to predict future temporal trends, frequency, distribution, and amounts of rainfall in relation to ET_o so as to develop effective irrigation management strategies. Little research has been conducted in this region, however. One study assessed spatial rainfall variability in multiple states at a regional scale (Dyer and Mercer 2013) and found there to be considerable spatial variability and substantial inconsistency in rainfall patterns, but the researchers stressed that their results could only be used in a general sense. Therefore, our study has focused on time series analysis of long-term weather records to evaluate rainfall, ET_o, and water deficit at the local scale in an effort to make more accurate predictions in the future for this specific area.

The Mann–Kendall (MK) and Kendall methods (Kendall and Gibsons 1990) have been widely used and tested as common and effective methods to evaluate the presence of a statistically significant trend in climatological and hydrological time series (Birsan et al. 2005; Norrant and Douguedroit 2006). The linearly fitted, nonparametric model does not require any hypotheses on a specific distribution of the variables (i.e., normal distribution), and data outliers do not affect the results (Renard et al. 2006). This study applied the MK method to analyze a long-term time series of weather data from a weather station located in the eastern Blackland Prairie for the 1894–2014 time period. The purpose of this paper is to model and characterize monthly, seasonal, and annual distribution patterns, trends, and temporal variability in rainfall, ET_o, and water deficit to aid local professionals and producers who rely on data from this weather station in improving water-management practices for greater water-use efficiency.

2. Data and methods

a. *Historical weather data*

Historical weather data in the Black Prairie region were assembled for the time period from 1894 to 2014. Data from weather stations near Macon (latitude 33.1°, longitude 88.6°, and elevation 60 m) were selected for the analysis. Weather data, including daily precipitation and maximum and minimum air temperature, were obtained online (http://ext.msstate.edu/anr/drec/; https://beaumont.tamu.edu/climaticdata/StateMap.aspx?index=2_14_0_26&name=MISSISSIPPI; http://www.wcc.nrcs.usda.gov/nwcc/site?sitenum=2174&state=al). Precipitation was measured by a tipping-bucket rain gauge (Texas Electronics, Inc., TR-525), and air temperature was measured by thermocouple temperature probes with naturally aspirated shields (Campbell Scientific, Inc., 107LC). The data quality of the long-term air temperature and precipitation was checked with quality-control procedures recommended by Allen et al. (1998) prior to use.

b. ET_o *calculation method*

Many methods have been proposed and are in use to estimate daily reference evapotranspiration. The methods

range from simple empirical equations to sophisticated energy- and mass-transfer models. The de facto standard method is that described by Allen et al. (1998), referred to as the FAO-56 Penman–Monteith, or FAO-56 method, but it requires several weather parameters that are often not routinely measured and are largely unavailable in historical weather records. Many studies have been undertaken around the world to evaluate alternative methods of estimating ET_o using more readily available weather data when the complete weather dataset required for using the FAO-56 method is not available. In the humid southeastern region of the United States, where the Black Prairie and the state of Mississippi are located, several studies were undertaken to evaluate alternative ET_o methods. Lu et al. (2005) and Yoder et al. (2005) evaluated several alternative ET_o methods and concluded that the method developed by Turc (1961) was superior to other empirical methods. Fisher and Pringle (2013) evaluated the Turc method against two alternative ET_o methods recommended by Allen et al. (1998) when use of the FAO-56 method was not feasible for six weather stations across Mississippi. Because their objective was to evaluate ET_o estimates that are based only on air temperature, the Turc equation was used with measured air temperature and estimated solar radiation, yet it performed better than the recommended alternative methods.

The Turc equation, on the basis of its performance under humid conditions and the limited availability of weather data, was chosen for estimation of ET_o in this study. Because reliable measurements of only air temperature were available for the entire time period under study, the method described by Fisher and Pringle (2013)—which uses measured air temperature and estimated, rather than measured, solar radiation—was used. This method is described in the following series of equations.

Reference evapotranspiration is estimated as

$$\mathrm{ET}_o = 0.0133\left(\frac{T_{\mathrm{mean}}}{T_{\mathrm{mean}}+15}\right)(23.8856R_s + 50), \quad (1)$$

where ET_o is reference evapotranspiration (mm day^{-1}), R_s is solar radiation (MJ m^{-2}), and T_{mean} is average air temperature (°C); T_{mean} is calculated as $(T_{\max} + T_{\min})/2$, where $T_{\max}$ and $T_{\min}$ are measured daily maximum and minimum air temperatures (°C), respectively. Solar radiation is estimated using the Hargreaves and Samani (1982) method and is calculated as

$$R_s = 0.16(T_{\max} - T_{\min})^{0.5}R_a, \quad (2)$$

where R_a is extraterrestrial radiation (MJ m^{-2}), which is a theoretical estimate of the radiation striking a point on Earth given that point's latitude and the day of the year. It is estimated as

$$R_a = \frac{24(60)}{\pi}G_{\mathrm{sc}}d_r[\omega_s\sin(\phi)\sin(\delta) + \cos(\phi)\cos(\delta)\sin(\omega_s)], \quad (3)$$

where G_{sc} is the global solar constant (0.0820 MJ m^{-2} min^{-1}) and ϕ is latitude (radians), with degrees of latitude converted to radians [radians = degrees × (π/180)]. The remaining factors in Eq. (3) are then calculated on the basis of calendar day:

$$d_r = 1 + 0.33\cos\left(\frac{2\pi}{365}J\right), \quad (4)$$

where d_r is inverse relative distance from Earth to the sun and J is calendar day,

$$\delta = 0.409\sin\left(\frac{2\pi}{365}J - 1.39\right), \quad (5)$$

where δ is solar declination (radians), and

$$\omega_s = \arccos[-\tan(\phi)\tan(\delta)], \quad (6)$$

where ω_s is sunset hour angle (radians).

The Hargreaves and Samani solar radiation model [Eq. (2)], recommended for use by Allen et al. (1998) when R_s measurements are unavailable, has been evaluated extensively [e.g., by Liu et al. (2009)] and was found to provide estimates with accuracy that is similar to that of other, more-complex radiation models. Fisher and Pringle (2013) evaluated the model on a daily basis using long-term data measured across Mississippi. They found solar radiation estimates to agree well with measured radiation, with average errors in daily estimates ranging from −3.0% to 4.1% among six locations and slopes of the regression lines between measured and estimated solar radiation that are close to 1.0, ranging from 0.91 to 1.09.

c. *Rainfall deficit*

Water deficit is often classified as a meteorological, hydrological, and/or agricultural deficit (Mishra and Singh 2010). Different indices have been proposed, such as the Palmer drought severity index (Palmer 1965), standardized precipitation index (McKee et al. 1993), soil moisture drought index (Hollinger et al. 1993), crop moisture index (Palmer 1968), and dryness index (DI; Arora 2002; Budyko 1974). Among these indices, DI, which is the ratio of ET_o to precipitation P, is useful for classifying the type of climate in relation to the water availability and has been utilized for many purposes,

including estimation of runoff in different regions of the world (Arora 2002; Gao and Giorgi 2008; Li et al. 2012; Nastos et al. 2013). The advantage of this index is that it is feasible to convert to any vegetation or crop deficit index using DI multiplied by the crop coefficient K_c. Therefore, it is a universal index that can serve many purposes in different research areas. Note, however, that DI is not valid when P is 0, which is highly likely within short time intervals, and therefore it is best suited for annual, seasonal, or monthly indices. The dryness index is given by

$$\mathrm{DI} = \mathrm{ET}_o/P. \tag{7}$$

In addition, the difference between rainfall and ET_o is often used for water-management purposes. When the difference is negative, rainfall is less than evapotranspiration, and the rainfall deficit RD is a negative value. When rainfall exceeds evapotranspiration, the difference is referred to as a rain surplus (RS). The two quantities are respectively given by

$$\mathrm{RD} = P - \mathrm{ET}_o, \quad P < \mathrm{ET}_o, \quad \text{and} \tag{8}$$

$$\mathrm{RS} = P - \mathrm{ET}_o, \quad P > \mathrm{ET}_o. \tag{9}$$

d. Temporal-trend analysis method

Locally weighted scatterplot smoothing ("LOWESS") was used to fit a smooth line to the time series data over time. This method guards against deviant points in the time series and allows us to see the trend of the data (Cleveland 1979). LOWESS estimates the mean through a nonparametric, robust local regression of the time series data using a weight function. Smoothness of the fit increases as the fraction of the data used to compute the mean at each abscissa value increases. The MK rank-based nonparametric method was used to detect statistically significant trends over time. The MK statistic S, the variance of the MK statistic $\mathrm{Var}(S)$, and the associated standard normal test statistic Z_{MK} are calculated as follows (Li et al. 2012):

$$S = \sum_{i=1}^{n-1} \sum_{j=i+1}^{n} \mathrm{sgn}(X_j - X_i), \quad \text{where} \tag{10}$$

$$\mathrm{sgn}(X_j - X_i) = \begin{cases} +1 & \text{if} \quad (X_j - X_i) > 0 \\ 0 & \text{if} \quad (X_j - X_i) = 0 \\ -1 & \text{if} \quad (X_j - X_i) < 0 \end{cases}, \tag{11}$$

$$\mathrm{Var}(S) = \frac{1}{18}\left[n(n-1)(2n+5) - \sum_{p=1}^{q} t_p(t_p-1)(2t_p+5)\right], \tag{12}$$

and

$$Z_{\mathrm{MK}} = \begin{cases} \dfrac{S-1}{\sqrt{\mathrm{Var}(S)}} & \text{if} \quad S > 0 \\ 0 & \text{if} \quad S = 0 \\ \dfrac{S+1}{\sqrt{\mathrm{Var}(S)}} & \text{if} \quad S < 0 \end{cases}. \tag{13}$$

In Eq. (10), X_i and X_j are the time series observations in chronological order, n is the length of the time series, and $\mathrm{sgn}(X_j - X_i)$ is the sign function, which returns only the sign of the difference (either positive or negative). In the variance calculation, q is the number of tied groups and t_p is the number of data values in the pth group, where p sums from 1 to q, the total number of tied groups. A tied group is a set of sample data having the same value. Positive values of Z_{MK} indicate increasing trends, and negative Z_{MK} indicates decreasing trends. At the significance level $\alpha = 0.05$, if $|Z| > Z_{1-(\alpha/2)}$, then the null hypothesis that there is no significant trend is rejected and a significant trend exists in the time series. The critical value of $Z_{1-(\alpha/2)}$ for the significance level $\alpha = 0.05$ is 1.96.

The direction and magnitude of the trend in time series data were quantified using Sen's slope, or b (Sen 1968). To derive an estimate of the slope b, the slopes of all data pairs are calculated by

$$b_i = \frac{X_j - X_i}{j - i}, \quad i = 1, 2, \ldots, N, \quad j > i. \tag{14}$$

The Sen's estimator of the slope is the median of these N values of b_i:

$$b = \begin{cases} b_{(N+1)/2} & \text{if} \quad N \text{ is odd} \\ 0.5[b_{N/2} + b_{(N+2)/2}] & \text{if} \quad N \text{ is even} \end{cases}. \tag{15}$$

The sign of b reflects the direction of trend in the data, and its value represents the steepness of the trend.

The MK test requires that a time series be serially independent. The trend-free prewhitening (TFPW) approach was applied to eliminate serial correlations in the time series data, if they existed, so as to conform to this requirement. This was done with the "R" software package using the Yue and Pilon method (Bronaugh and Werner 2013). In this method, the slopes were estimated using the Theil–Sen approach. If the slope is almost equal to zero, then it is not necessary to conduct the trend analysis. If the slope differs from zero, then it is assumed to be linear and the data are detrended by the slope; the autoregressive model of order 1 [AR(1)] is then computed for the detrended series. An explanation of AR(1) is detailed in section 2e. The residuals should be an independent series, and

then the trend and residuals are blended together. Last, the MK test is applied to the combined series to assess the significance of the trend. Once the MK test was applied to the data, if there existed a significant trend at the 95% level ($\alpha = 0.05$), the sequential MK (SQMK) test was applied to detect possible shifts in trends. When either the progressive row or the retrograde row exceeds the confidence limits before and after the crossing points, this trend turning point is considered to be significant.

e. Forecast models

Autoregressive, integrated, and moving-average (ARIMA) modeling was applied to forecast the time series data for the period of 2015–24. ARIMA modeling predicts future values as a product of several past observations and random errors (Yürekli et al. 2007). The model has an effect of smoothing (noise reduction) to observe underlying fluctuation trends (Shumway and Stoffer 2011) and is applicable to data that are stationary in the mean and variance. The autoregressive method regresses the current time point on previous values, known as time-lagged values of the forecast variable. This approach assumes that the future can be explained by the past because of the autocorrelation between the future and past, which is useful for forecasting. The integrated part of the model accounts for trends using differencing; if there is any nonstationarity, the model will include some level of differencing. The moving-average (MA) part of the method models the relationship between the noise variation and the current observed data point. These models are written as ARIMA(p, d, q), where p is the number of autoregressive lags, d is the order of differencing, and q is the number of moving-average lags. These numbers help to forecast and detect trends, dependence, and seasonality in the data (Makridakis et al. 1998).

These models can be extended to account for seasonal fluctuations, with the expression ARIMA(p, d, q)(P, D, Q)$_s$, where s is the length of the seasonal period. If $s = 12$, the length of the seasonal period is annual. The parameters P, D, and Q are the number of seasonal autoregressive terms, number of seasonal differences, and number of seasonal moving averages, respectively. The modeling process includes model identification and diagnostic checking. The model identification is performed by determining the appropriate values for p, d, and q and for P, D, and Q. For each dataset of rainfall, ET$_o$, or DI, multiple candidate models were identified. A parsimonious model selection was based on diagnostic checking, including the use of the Akaike information criterion (AIC) that penalizes the number of parameters in a model. The more parameters that there are in a model, the better is the fit, but the model will not have any explanatory power if there are too many parameters. AIC is useful because it explicitly penalizes any extra parameters in the model, by adding $2(p + 1)$ to the deviance. When comparing models, the model with the smallest AIC will be the better fit for the data (Akaike 1974). The residuals were also checked to make sure that they were independent with equal variance and followed a normal distribution.

f. Validation criteria of model performance

Statistical measures, including mean, standard deviation (STDev), root-mean-square error (RMSE) normalized to the mean of the observed values (RRMSE), mean absolute error (MAE) normalized to the mean of the observed values (RMAE), ratio of RMSE to the standard deviation of observed data (RSR), average percent bias (PBIAS), Nash–Sutcliffe modeling efficiency (EF), and index of agreement D, were used to evaluate model performance (Legates and McCabe 1999; Moriasi et al. 2007; Ahuja and Ma 2002; Ma et al. 2011, 2012).

RMSE normalized to the mean of the observed values is calculated as

$$\mathrm{RRMSE} = \left[\frac{1}{N}\sum_{i=1}^{N} w_i(P_i - O_i)^2\right]^{1/2} \Big/ \overline{O}, \qquad (16)$$

where w_i is the weight factor (often set equal to 1.0); P_i and O_i are the model-predicted and experimentally observed points, respectively; $\overline{\mathrm{O}}$ is the mean observed value; and N is the number of observed data points. The RRMSE reflects the difference in mean values between the experimental and simulated results for a dataset with N measured points. The smaller the value of RRMSE is, the better is the validation. The ratio of RMSE to the standard deviation of measured data is calculated as

$$\mathrm{RSR} = \left[\sum_{i=1}^{N}\frac{1}{N}(P_i - O_i)^2\right]^{1/2} \Big/ \left[\sum_{i=1}^{N}\frac{1}{N}(O_i - \overline{O})^2\right]^{1/2}. \qquad (17)$$

MAE is defined as

$$\mathrm{MAE} = \sum_{i=1}^{N} |P_i - O_i|/N. \qquad (18)$$

Similar to RRMSE, the relative MAE is calculated as

$$\mathrm{RMAE} = \mathrm{MAE}/\overline{O}. \qquad (19)$$

TABLE 1. Summary of rainfall (mm) statistics for the study station: standard deviation (SD), skewness C_s, kurtosis C_k, minimum value (Min), maximum value (Max), and coefficient of variation (CV).

Time	Mean	Median	SD	C_s	C_k	Min	Max	CV
Annual	1307.21	1283.03	364.95	0.28	−0.28	660.14	1959.13	0.20
Winter	385.72	378.98	119.67	0.34	−0.33	170.96	708.11	0.31
Spring	370.68	351.49	136.91	0.84	0.47	104.64	820.17	0.37
Summer	297.44	288.29	106.96	0.47	0.36	100.08	696.24	0.36
Autumn	253.37	242.56	121.02	0.74	0.20	46.99	654.31	0.48
Jan	130.66	121.16	66.04	0.84	0.82	13.46	369.07	0.51
Feb	130.81	122.42	64.54	0.66	−0.12	32.01	309.11	0.49
Mar	143.54	133.86	75.38	1.00	1.61	10.91	432.80	0.53
Apr	125.56	110.24	79.05	0.85	0.39	6.35	380.24	0.63
May	101.58	84.59	63.16	0.96	0.82	6.35	329.94	0.62
Jun	91.61	83.85	59.41	1.27	2.46	3.56	353.56	0.65
Jul	118.43	108.45	66.70	1.11	1.26	11.68	354.58	0.56
Aug	87.40	84.07	53.53	0.36	−0.72	0.00	220.74	0.61
Sep	82.71	71.12	60.97	1.08	0.99	0.00	296.68	0.73
Oct	72.03	54.86	58.74	1.19	1.12	0.00	270.00	0.82
Nov	98.63	90.17	63.50	1.14	1.67	0.00	354.13	0.64
Dec	125.62	116.57	68.12	1.09	1.55	7.87	369.04	0.54

Smaller RMAE values indicate better performance of a model. The percent bias is calculated as

$$\text{PBIAS} = 100\% \times \sum_{i=1}^{N} (P_i - O_i) \Big/ \sum_{i=1}^{N} O_i. \quad (20)$$

Modeling efficiency is calculated as

$$\text{EF} = 1.0 - \left[\sum_{i=1}^{N} (P_i - O_i)^2 \Big/ \sum_{i=1}^{N} (O_i - \overline{O})^2 \right]. \quad (21)$$

The EF is a measure of the deviation between model simulations and observations in relation to the scattering of the observed data. A value of EF = 1 indicates a perfect match between predictions and measurements. A high EF indicates good agreement between simulated and measured values. The index of agreement is defined as

$$D = 1.0 - \frac{\sum_{i=1}^{N} (P_i - O_i)^2}{\sum_{i=1}^{N} (|P_i - \overline{O}| + |O_i - \overline{O}|)^2}. \quad (22)$$

Note that D is more sensitive than traditional correlation measures to differences between observed and predicted means and variances. Index D varies from 0 to 1.0, with higher values indicating better fit (Legates and McCabe 1999), and $D = 1$ means perfect simulation.

Moriasi et al. (2007) suggested that multiple statistics should be used in model validation to avoid biases. Therefore, all of the above statistic parameters were calculated for evaluation of our fitted models.

3. Results and discussion

a. Preliminary analysis

1) RAINFALL

The preliminary analysis for this study included computing the mean, median, standard deviation, coefficient of skewness, coefficient of kurtosis, and coefficient of variation (CV) in the precipitation, ET_o, and DI time series. Table 1 presents these summary statistics for the 120-yr time period studied (1894–2014). The mean for annual rainfall was 1307 mm, and annual rainfall varied from 660 to 1959 mm, with 55 of 120 years receiving rainfall above the mean value. The data were slightly skewed, with almost one-half of the years receiving annual rainfall below the mean. Mean rainfall for the different seasons ranged from 253 to 386 mm, and monthly average rainfall varied from 72 to 144 mm over the 12 months of the year. Most rainfall occurred in winter (December–February) and spring (March–May): only 23% of total rainfall occurred in summer (June–August), and 37% occurred during the crop-growing season, from May to September. These results are in agreement with the conclusions that high rainfall normally occurred in the cool seasons with more consistency than in the warm seasons in Mississippi (Dyer and Mercer 2013). The maximum difference between mean and median values was less than 20 mm, suggesting that there were few outliers. Rainfall is positively skewed at all temporal scales and is generally more skewed after March, except for August. More-skewed months have more rainfall events, and those events have lighter rainfall.

TABLE 2. As in Table 1, but for ET_o (mm).

Time	Mean	Median	SD	C_s	C_k	Min	Max	CV
Annual	1209.94	1215.32	53.20	0.20	−0.16	1101.15	1372.08	0.04
Winter	128.30	128.63	19.98	−0.03	0.31	82.15	183.16	0.13
Spring	350.37	349.48	18.90	0.75	2.17	310.53	436.27	0.05
Summer	457.66	456.39	24.22	0.47	0.20	409.16	537.66	0.05
Autumn	273.62	271.59	17.48	0.23	−0.68	235.19	311.42	0.06
Jan	40.45	40.35	7.72	−0.01	−0.36	21.21	60.35	0.19
Feb	49.30	49.34	9.54	0.10	0.63	19.30	81.45	0.19
Mar	86.80	85.74	11.30	0.12	0.22	56.27	120.08	0.13
Apr	117.31	116.34	7.79	0.29	0.40	97.52	145.47	0.07
May	146.26	145.74	8.62	0.40	1.16	124.39	181.28	0.06
Jun	153.68	151.94	10.43	0.34	−0.60	128.95	176.84	0.07
Jul	156.60	156.17	10.33	0.51	0.37	135.77	191.39	0.07
Aug	147.38	146.96	8.98	0.38	−0.12	127.12	172.54	0.06
Sep	122.09	120.56	8.76	0.19	−0.67	103.71	142.92	0.07
Oct	94.12	93.48	7.64	−0.01	−0.60	76.77	109.83	0.08
Nov	57.41	56.90	6.35	0.21	−0.38	42.44	74.35	0.11
Dec	38.85	38.99	6.88	0.05	1.25	14.65	60.78	0.18

The coefficient of variation, a measure of dispersion around the mean, was also calculated to analyze the variability of the time series data. Coefficients of variation for annual and seasonal rainfall were low, but the coefficients for monthly rainfall were high, ranging from 0.49 to 0.82 over the 12 months. Large variation coefficients and ranges of annual, seasonal, and monthly rainfall, especially during the months of crop growth, indicate that rainfall is a highly variable climatic factor. The considerable variations present greater challenges for water management—in particular, at field scales.

2) ET_O

Table 2 shows ET_o values and statistics for annual, seasonal, and monthly time periods. Mean annual ET_o was 1210 mm, and annual ET_o varied from 1101 to 1372 mm. Coefficient of variation and standard deviation were only 4% (CV value × 100) and 53 mm, respectively. Annual ET_o of one-half of the 120 years was below the mean annual ET_o, but maximum annual ET_o was only 162 mm greater than the mean. The range of ET_o is much less than that of rainfall (Table 1). Unlike rainfall, ET_o did not show much variation over the years, which implies that success in rain-fed agriculture depends more on rainfall than on ET_o. As expected, mean ET_o was the highest in summer, followed by spring, autumn, and winter. Mean monthly ET_o for the months during the crop-growing season (April–September) ranged from 117 to 157 mm, and mean rainfall ranged from 83 to 126 mm for those same months.

3) WATER DEFICIT AND DI

Annual mean rain "deficit" (the difference between rainfall and ET_o) was 97 mm, with the positive value indicating that there was a rainfall surplus rather than a deficit. The annual rain deficit/surplus ranged from −602 to 795 mm (Fig. 1c). The mean of annual rain surplus was 271 mm, and the surplus varied from 10 to 795 mm. Surplus years accounted for 60% of the time period of 120 years. Only 48 of the 120 years had a rain deficit on an annual temporal scale. It was found that 1896, 1901, 1903, 1904, 1907, 1910, 1921, 1924, 1952, 1954, 1958, 1978, 1981, 2000, and 2007 experienced annual deficits of more than 200 mm, which resulted in severe-drought conditions during crop-growing seasons. The rain deficit in summer was as high as 160 mm, and the monthly rain deficit ranged from −22 to −62 mm during the crop-growing season from May to October. Even larger deficits of rainwater can often be observed at shorter time periods such as weekly intervals. This suggests that rainfall often cannot meet crop water requirements in the region and that supplemental irrigation is required to stabilize or maximize crop productivity.

Arora (2002) categorized climatic regimes into four groups: arid ($12 > DI \geq 5$), semiarid ($5 > DI \geq 2$), subhumid ($2 > DI \geq 0.75$), and humid ($0.75 > DI \geq 0.375$). Table 3 shows that mean annual DI was 0.97 and mean seasonal DI ranged from 0.37 to 1.8 over the four seasons, which suggest that the study area is in a subhumid region. Dryness index as a ratio of ET_o to rainfall is helpful in determining the deficit of rainfall for meeting crop water requirements and the need for irrigation. Large monthly DI values with considerable variation are found in summer and in the months of crop growing from April to October. DI values ranged from less than 2 to almost 5, with great variability throughout critical water-requirement stages of crop growth, classifying these time periods in the semiarid category for the subhumid region.

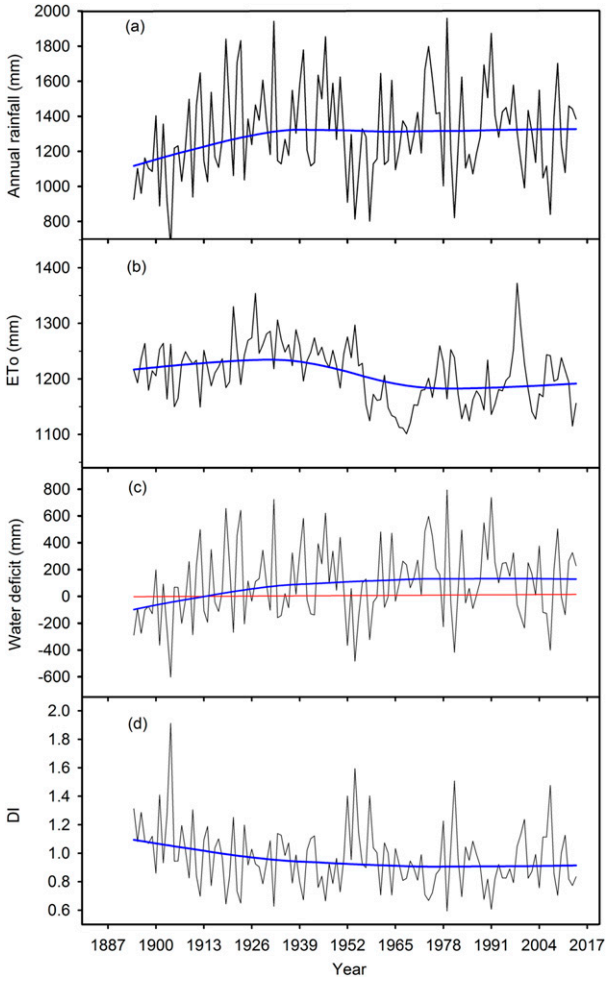

FIG. 1. Historical time series data and LOWESS curve trend (blue curves) in (a) annual rainfall, (b) ET_o, (c) rainfall deficit, and (d) DI from 1894 to 2014.

b. *Historical time series trend characteristics*

1) ANNUAL AND SEASONAL TRENDS

(*i*) *Annual trend*

LOWESS curves (Helsel and Hirsch 2002) were fit to the time series data. Figure 1 illustrates historical time series data along with LOWESS curve trends in annual rainfall, ET_o, water deficit, and DI from 1894 to 2014. Rainfall varied substantially around the mean with the LOWESS curve for annual rainfall (Fig. 1a), showing an increasing trend in rainfall from 1894 to 1934, after which the rainfall trend became stationary. Overall, the curve that is based on annual data suggests an increasing trend. LOWESS curves are used to show patterns and do not explain statistically significant trends in the time series. Therefore, the MK test was performed.

TABLE 3. As in Table 1, but for DI.

Time	Mean	Median	SD	C_s	C_k	Min	Max	CV
Annual	0.97	0.95	0.22	1.04	2.04	0.59	1.19	0.22
Winter	0.37	0.34	0.13	1.27	1.60	0.20	0.89	0.37
Spring	1.09	1.01	0.46	1.87	6.93	0.39	3.63	0.42
Summer	1.80	1.61	0.84	1.52	2.48	0.63	5.09	0.47
Autumn	1.43	1.13	0.96	2.27	6.62	0.40	6.25	0.67
Jan	0.44	0.33	0.47	5.83	44.48	0.10	4.48	1.06
Feb	0.50	0.38	0.32	1.95	5.00	0.15	1.96	0.65
Mar	0.97	0.60	1.30	4.76	25.08	0.20	9.17	1.34
Apr	1.76	1.05	2.36	4.73	30.12	0.29	20.22	1.34
May	2.54	1.67	3.16	4.38	23.70	0.44	24.99	1.24
Jun	3.24	1.84	5.10	5.89	42.39	0.40	46.29	1.58
Jul	2.01	1.43	2.00	3.70	15.91	0.38	13.90	0.99
Aug	3.65	1.75	7.06	5.96	42.85	0.00	63.51	1.94
Sep	4.67	1.61	11.59	5.11	27.62	0.00	83.95	2.48
Oct	4.89	1.50	14.65	6.64	47.84	0.00	128.37	2.99
Nov	0.99	0.62	1.06	3.08	12.73	0.00	7.68	1.07
Dec	0.48	0.34	0.61	5.20	30.78	0.10	4.79	1.27

The magnitude of statistically significant trends was determined using Sen's slope estimator. The calculated MK statistics Z_{MK} and the Sen's slope b of seasonal and annual rainfall, ET_o, rainfall deficit, and DI are shown in Table 4, and monthly values are shown in Table 5. The tests did not show the increasing trend in annual rainfall to be statistically significant. Roderick et al. (2009a,b) found an increasing trend in mean annual rainfall in North America, and Karl et al. (2009) reported that precipitation had increased by an average of about 5% over the past 50 years in the United States. Liu et al. (2012) also found that annual rainfall had increased slightly over time across the midsouthern United States, with the neighboring state of Tennessee exhibiting the most significant increase in annual precipitation.

There appeared to be an increasing trend in ET_o from 1894 to 1934, after which ET_o decreased until 1968, and then it increased slightly again. For trends that were significant according to the MK test at the 95% confidence level, the SQMK test was applied to analyze potential

TABLE 4. Mann–Kendall statistical test result Z_{MK} and Sen's slope b of seasonal and annual rainfall P, ET_o, rain deficit (RD) or rain surplus (RS), and DI. An asterisk denotes significance at a confidence level of 95%.

	Test	Winter	Spring	Summer	Autumn	Annual
P	Z_{MK}	0.02	−0.02	0.04	0.23*	0.11
	b	0.08	−0.11	0.19	1.06*	1.17
ET_o	Z_{MK}	−0.04	−0.06	−0.03*	−0.22*	−0.15
	b	−0.01	−0.08	−0.29*	−0.18*	−0.51
RD/RS	Z_{MK}	0.01	−0.02	0.08	0.24*	0.15*
	b	0.07	−0.11	0.45	1.21*	1.80*
DI	Z_{MK}	0.00	0.02	−0.05	−0.23*	−0.13*
	b	0.000	0.000	−0.002	−0.006*	−0.001*

TABLE 5. The Z_{MK} and b of monthly P, ET_o, and DI in the last 10 decades. An asterisk denotes significance at a confidence level of 95%.

	Test	Jan	Feb	Mar	Apr	May	Jun	Jul	Aug	Sep	Oct	Nov	Dec
P	Z_{MK}	0.06	−0.01	−0.06	0.02	−0.05	0.004	0.003	0.08	0.14*	0.14	0.15	−0.03
	b	0.16	−0.03	−0.18	0.05	−0.08	0.007	0.01	0.24	0.35*	0.29	0.34	−0.07
ET_o	Z_{MK}	−0.13*	0.09	0.01	0.00	−0.16*	−0.25*	−0.23*	−0.19*	−0.26*	−0.13*	−0.07	−0.03
	b	−0.05*	0.03	0.00	0.00	−0.07*	−0.12*	−0.11*	−0.07*	−0.10*	−0.05*	−0.02	−0.01
DI	Z_{MK}	0.11	0.07	0.183	−0.014	0.095	0.013	0.094	0.135*	0.045	0.057	0.051	0.095
	b	0.010	0.008	0.038	−0.003	0.033	0.005	0.042	0.054*	0.011	0.009	0.004	0.010

significant shifts in the time series data. The test results revealed that the trend in ET_o shifted significantly around 1934 and shifted again from decreasing to increasing around 1968, but this latter trend was not significant. This decreasing trend in ET_o was also detected in North America by Burn and Hesch (2007) and Hobbins et al. (2004).

The pattern of annual rainfall deficit is similar to that of rainfall (Figs. 1a,c), suggesting that the trends were dependent more on precipitation than on evapotranspiration. In summer months, precipitation amounts are generally much smaller than the amounts involved in evapotranspiration. The rainfall deficit curve exhibits an upward trend in differences between rainfall and ET_o, beginning below 0, representing deficit (negative) values, and lasting until around 1917 (Fig. 1c). After 1917, a surplus trend is detected at an annual temporal scale in this region. The significant positive trend exhibits an increase in rain surplus of 1.8 mm annually, due mainly perhaps to large surplus values observed in the autumn season (Table 4).

The trends in annual DI significantly decreased by 0.001, resulting from increased rainfall and decreased ET_o. The reduced DI indicates a continuous relief of the rain deficit in the last eight decades. There is an indication of decreasing changepoints. From the LOWESS plot and the SQMK test, it is found that the annual decreasing DI trend significantly shifted in 1904, 1908, and 1926 at the 95% confidence level.

(*ii*) *Seasonal trends*

The MK and Sen's slope tests were also used to identify seasonal trends between 1894 and 2014. A mix of negative and positive trends was seen in different seasons (Table 4). Autocorrelation was only present for the autumn season of rainfall; therefore, the prewhitening method TFPW was applied to eliminate serial correlations before applying the MK test and Sen's slope estimator. A significant positive trend in rainfall at a confidence level of 95% was found in the autumn months, and rainfall increased by 1.06 mm each autumn season (Table 4). The slight increase is not very beneficial to crop production in this region because most crops are already harvested or mature in autumn. Liu et al. (2012) also projected that the climate is wetter in the region during autumn months. Although the trends in rainfall also increased slightly in summer and winter, they were not significant. A downward trend in spring was found, and the mean rainfall was as high as 371 mm in spring months, which is only 15 mm less than the highest-rainfall winter season. The wet spring in this region meant that growers had a very short time window for field operations and often delayed crop seeding, and therefore the decreasing trend in spring rainfall is actually good for agriculture production in the southeastern United States. The wet and mild winter in this region often causes significant runoff and leaching that could result in degradation of surface and groundwater quality. Therefore, some field activities that cannot be conducted in spring because of high and frequent rainfall and need to be performed in autumn are also limited because of the wet winter.

As expected, cumulative ET_o is the highest in summer, followed by spring, autumn, and winter (Fig. 2b). There were significant decreasing trends in the summer and autumn seasons, which primarily contributed to an overall decrease in annual ET_o of 0.51 mm. ET_o decreased by ~0.29 mm in summer and 0.18 mm in autumn (Table 4). Seasonal water deficit/surplus, shown in Fig. 2c, occurred mainly in summer, and winter had the highest water surplus. Water deficit/surplus was generally distributed around the 0 line in spring and autumn. Autumn was the only season that showed a slight autocorrelation, at lag 16; the remaining seasons showed no autocorrelation. There was a significant increasing trend in water deficit of 1.21 mm yr^{-1} for the autumn season. Rain deficit displayed a decreasing trend in spring, but it was not significant. In a similar way, the highest DI was observed in summer, followed by autumn, spring, and winter (Fig. 2d). A significant downward trend in DI was detected, with DI decreasing by 0.006 for the autumn season each year (Table 4). No significant shifts in DI trend for any other seasons were found.

2) MONTHLY TIME SERIES TRENDS

Significant autocorrelation was detected for rainfall in March, May, and August. There was also significant

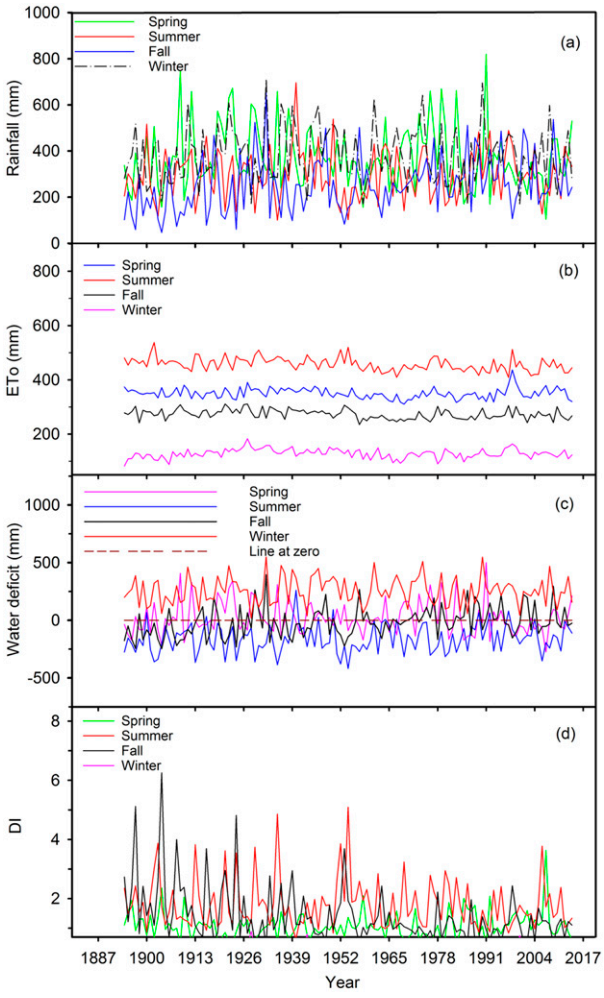

FIG. 2. Seasonal (a) rainfall, (b) ET_o, (c) rainfall deficit, and (d) DI from 1894 to 2014.

autocorrelation for ET_o in January, February, May, June, July, September, and October. The autocorrelations were removed using the prewhitening method. The MK test was applied on a monthly scale to detect trends in the rainfall series and showed a mix of positive and negative trends in different months. A significant upward trend in September at a confidence level of 95% was observed (Table 5), and rainfall was significantly increased by 0.35 mm each September, which greatly contributed to the increasing trend in the autumn season. A slight decrease in rainfall was detected for February, March, May, and December, although it was not significant, which implies that those months were trending generally toward drier conditions.

Table 5 highlights some significant small decreasing trends in ET_o for the months of January, February, May, June, July, August, September, and October. The decreasing trends during these months contributed to the significant decreases in ET_o in summer and autumn. The monthly trend test found a significant increasing trend in DI only for August. The DI increased about 0.054 for this month each year. DI for all months except April increased, although the increase was not significant (Table 5).

c. *Forecast models*

1) ANNUAL FORECAST MODELS

(*i*) *Annual rainfall forecast and validation*

From the autocorrelation function (ACF) and partial autocorrelation function (PACF) plots, it was observed that annual rainfall was autocorrelated between years. We removed the trend (seasonal, cyclic, or other trends) by differencing the data, and then we classified the type of model once the data were stationary in the mean and variance. This process was repeated, and different models were tested to come up with the best-fit ARIMA model for the data that would allow us to account for trend and seasonality and, ultimately, to forecast future trends.

The best-fit model, ARIMA(0, 1, 1), was chosen for prediction of annual rainfall. This model includes a moving-average component with lag-1 MA(1), indicating that forecasting can be done using the residuals of the previous time point observed. Forecasting is dependent on one step before, which suggests that the model is able to give accurate insight for 1 year ahead since the prediction of annual rainfall in the next year is dependent on the estimated values in the previous year. Figure 3a shows that the ARIMA(0, 1, 1) model forecast 1319 mm of mean annual rainfall, with 775 and 1862 mm being the low and high levels of the 95% confidence interval for the next 10 years. The forecast annual rainfall was 1307 mm in 2015, which is only 22 mm higher than observed values (Table 6). The plot of the observed versus predicted rainfall also verified that the ARIMA(0, 1, 1) is a good fit for prediction (Fig. 3a). Mean measured and predicted annual rainfall amounts from 1894 to 2014 were 1307 and 1286 mm, respectively. RRMSE, RMAE, and PBIAS were 0.20, 0.16, and −0.01, respectively. Those low values indicate that the predicted estimates are very close to the measured values.

(*ii*) *Annual* ET_o *forecast and validation*

The ARIMA(1, 1, 1)(2, 1, 0)$_{-15}$ was selected as the model for prediction of annual ET_o. Predicted annual ET_o from 2015 to 2024 ranged from 1168 to 1242 mm, with 1061 and 1368 mm being the low and high levels of the 95% confidence interval (Fig. 3b). The forecast annual ET_o (1169 mm) was in near-perfect agreement with measured ET_o (1166 mm) in 2015 (Table 6). Both mean measured and predicted annual ET_o amounts from 1894

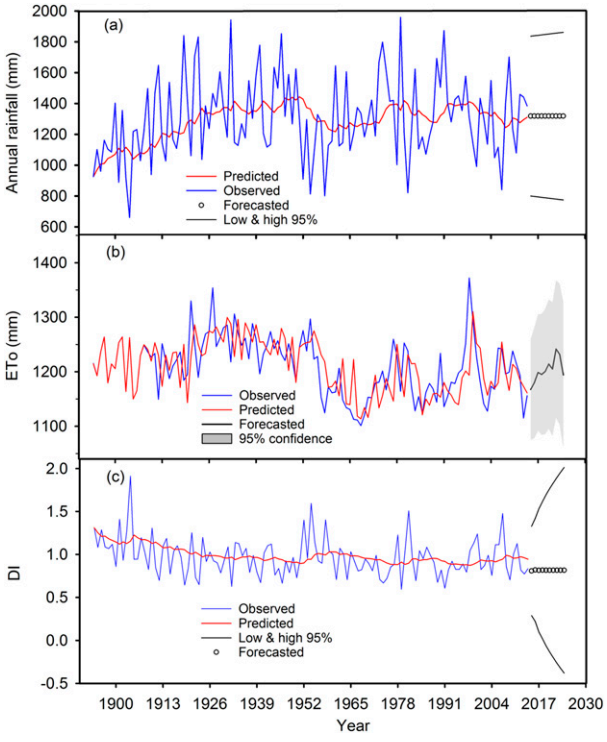

FIG. 3. Observed data and simulated and forecast annual (a) rainfall by a fitted ARIMA(0, 1, 1) model, (b) ET_o by a fitted ARIMA$(1,1,1)(2,1,0)_{-15}$ model, and (c) DI by a fitted ARIMA(1, 1, 0) model for the next 10 years after 2015.

to 2014 were close to 1210 mm. RRMSE, RMAE, PBIAS, EF, and *D* were 0.04, 0.03, 0.00, 0.84, and 0.96, respectively. Low values of RRMSE, RMAE, and PBIAS and high values of EF and *D* indicate that the model-predicted ET_o was very close to the measured values.

(*iii*) *Annual DI forecast and validation*

After examining diagnostics such as ACF residual plots, "qqnorm" plots for normality check, AIC, and the Bayes information criterion, it was determined that the ARIMA(1, 1, 0) is the best-fit model and can be used to predict DI for the next 10 years. Figure 3c shows that the ARIMA(1, 1, 0) model predicted 0.82 of mean annual DI with 0.02 and 2.0 being the low and high levels of the 95% confidence interval. Figure 3c shows that the actual DI values fall within the 95% confidence intervals. Although the point estimates for the forecast values are not as close to the actual values, the predicted values, in general, follow the pattern of observed values although its peak is, sometimes, a little bit ahead of the observed peak. The difference in annual DI between measured and forecast value in 2015 was only 0.03 (Table 6). Mean measured and predicted annual DIs from 1894 to 2014 were 0.97 and 0.99, respectively. RRMSE, RMAE, and PBIAS are 0.23, 0.17, and 0.02, respectively. The EF and *D* are as high as 1.0. These statistical indices indicate good agreement between observed and predicted values.

2) MONTHLY FORECAST MODELS

(*i*) *Monthly rainfall forecast*

Similar diagnostics and model-fitting exercises were conducted for the monthly rainfall data. Significant autocorrelations at lag 1 and 12 were found, showing

TABLE 6. Comparison of observed and forecast monthly rainfall, ET_o, and DI in 2015, with associated statistics.

	Rainfall (mm)		ET_o (mm)		DI	
	Measured	Forecast	Measured	Forecast	Measured	Forecast
Jan	157.48	129.56	38.48	36.98	0.24	0.33
Feb	126.49	128.66	32.60	47.85	0.26	0.43
Mar	136.40	139.04	83.05	85.69	0.61	0.75
Apr	134.40	124.78	112.47	114.12	0.84	1.14
May	86.61	99.48	140.37	142.71	1.62	1.83
Jun	43.94	91.29	144.31	148.06	3.28	2.08
Jul	133.09	117.31	158.38	150.88	1.19	1.55
Aug	108.46	89.37	143.43	143.43	1.32	1.92
Sep	37.08	85.96	118.35	117.47	3.19	3.63
Oct	70.39	75.72	86.84	90.90	1.23	1.57
Nov	112.77	102.09	56.92	54.50	0.50	0.64
Dec	138.36	123.29	50.30	36.41	0.36	0.36
Annual	1285.47	1306.55	1165.50	1169.00	0.84	0.81
RRMSE	0.22		0.07		0.37	
RMAE	0.17		0.05		0.27	
PBIAS	0.14		0.03		0.91	
RSR	0.02		0.01		0.00	
D	1.00		1.00		1.00	
EF	1.00		1.00		1.00	

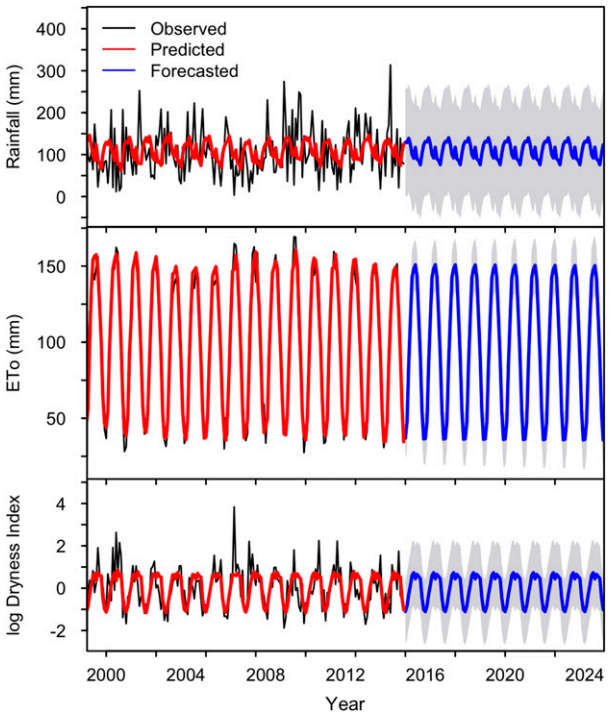

FIG. 4. Observed data and simulated and forecast monthly (top) rainfall by a fitted ARIMA$(1, 0, 1)(0, 1, 1)_{-12}$ model, (middle) ET_o by a fitted ARIMA$(1, 1, 2)(0, 1, 2)_{-12}$ model, and (bottom) logarithm of DI by a fitted ARIMA$(1, 0, 0)(0, 1, 1)$ model in the next 10 years after 2015.

seasonal behavior of the temporal pattern. Seasonal time series have a nonstationary mean, but the nonstationarity is of a regular kind; that is, every year or every month the cycle repeats. This type of time series can be represented using a model that explicitly allows for the seasonality. It was found that an ARIMA$(1, 0, 1)(0, 1, 1)_{-12}$ is the best fit for the model.

This model indicates a seasonal trend, resulting in the need to difference between the same time points between seasons (e.g., January one year differenced with January in the previous year, reflecting what was observed in the MK test). It also indicates a seasonal association (seasonality after accounting for trend) that suggests current rainfall behavior can be explained by the same month of last year's behavior ($Q = 1$) and by last month's rainfall ($q = 1$). This means that the use of recent observations would allow us to predict the future. Figure 4 displays the monthly forecast results for the next 10 years. The gray band is the 95% confidence interval for the forecast monthly rainfall.

(*ii*) *Monthly* ET_o *forecast*

From the ACF, PACF, differencing methods, and diagnostics, it was found that an ARIMA$(1, 1, 2)(0, 1, 2)_{-12}$ is the best-fit model of monthly ET_o, with smaller AIC and fewer parameters. This model has a seasonal difference of the original data, for a seasonal period of 12. It is capable of forecasting monthly ET_o for given years in the future. The monthly ET_o forecasts along with the 95% confidence interval for the next 10 years from 2015 to 2024 are exhibited in Fig. 4.

(*iii*) *Monthly DI forecast*

After examining the ACF and PACF plots, there is seasonality and a nonstationary mean that needs to be adjusted for in the data. We determined that an ARIMA $(1, 0, 0)(0, 1, 1)$ was the best-fit model; this model can be used to forecast DI for the next 10 years, as shown in Fig. 4.

(*iv*) *Validation of monthly forecast models*

Performance of the monthly forecast models was evaluated on the basis of the statistical indices: Moriasi et al. (2007) rated model performance as acceptable when EF > 0.5, $-25 <$ PBIAS < 25, and RSR < 0.7. Ahuja and Ma (2002) and Ma et al. (2011) suggested that a more stringent rating should be used for a point model: EF > 0.7, $-15 <$ PBIAS < 15, and RSR < 0.5. If RRMSE and RMAE are within 10% of the mean values of all measurements, it is a "very good" performance. Values of statistical indices for monthly rainfall, ET_o and DI observed from 1894 to 2014 are reported in Tables 7–9. The standard deviation of predicted rainfall, ET_o, and DI were much lower than the observed values. Both EF and D values of monthly rainfall, ET_o, and DI in each of 12 months are 1.0 (which indicates a perfect match between predictions and measurements), as were values of RRMSE, RMAE, PBIAS, and RSR for monthly predicted rain and ET_o (Tables 7–9).

At the conclusion of this study, monthly data for 2015 were not yet available. We are currently able to compare the data that were forecast at that time with the observed monthly data that are available now. Detailed results are presented in Table 6. The differences in monthly rainfall, ET_o, and DI between measured and forecast values ranged from 2 to 49 mm, from 0 to 15 mm, and from 0 to 1.2, respectively. All values of EF and D in 12 months reached 1.0 for rainfall, ET_o, and DI. The RRMSE and RMAE ranged from 0.05 to 0.37, that is, within 10% of the measured values of rainfall, ET_o, and DI. Values of PBIAS are within the criterion of ± 15, and RSR values were close to 0, much better than a satisfactory index of 0.5 (Table 6). All of those statistical performance indices suggest that the three forecast models are capable of predicting rainfall, ET_o, and DI with low values of standard deviation and root-mean-square error.

TABLE 7. Comparison of observed and predicted monthly rainfall from 1894 to 2014.

	Measured (mm)		Predicted (mm)							
	Mean	STDev	Mean	STDev	RRMSE	RMAE	EF	PBIAS	RSR	*D*
Jan	130.66	65.84	128.10	12.50	0.50	0.40	1.0	−0.01	0.06	1.0
Feb	130.81	64.54	132.65	8.84	0.50	0.40	1.0	0.01	0.06	1.0
Mar	143.54	75.38	148.32	8.36	0.52	0.40	1.0	0.03	0.07	1.0
Apr	125.56	79.05	118.79	18.05	0.62	0.48	1.0	−0.04	0.07	1.0
May	101.58	63.16	99.20	16.84	0.62	0.40	1.0	−0.02	0.05	1.0
Jun	91.61	59.41	96.35	12.26	0.64	0.49	1.0	0.04	0.05	1.0
Jul	118.43	66.70	115.32	10.80	0.57	0.43	1.0	−0.02	0.06	1.0
Aug	87.41	53.54	79.79	14.73	0.61	0.49	1.0	−0.07	0.04	1.0
Sep	82.71	60.97	73.63	10.95	0.74	0.44	1.0	−0.09	0.05	1.0
Oct	72.03	58.74	62.39	13.26	0.81	0.61	1.0	−0.11	0.05	1.0
Nov	98.63	63.50	85.93	17.44	0.64	0.46	1.0	−0.11	0.05	1.0
Dec	125.62	68.12	126.59	12.08	0.54	0.41	1.0	0.01	0.06	1.0

4. Conclusions

Sound water-management planning and cropping-system design can be achieved with an understanding of the statistical properties of long-term records of major climatic parameters such as rainfall and evapotranspiration. This study analyzed trends in monthly, seasonal, and annual precipitation, ET_o, and water deficit at a site in Macon, Noxubee County, in the Blackland Prairie of Mississippi over a 120-yr period (1894–2014). The mean observed annual rainfall was 1307 mm, varying from 660 to 1959 mm, with 37% of total rainfall occurring during the crop-growing season from May to September. Unlike rainfall, ET_o did not show significant variation with time. The mean annual ET_o was 1210 mm, and it varied from 1101 to 1372 mm. Monthly ET_o from April to September ranged from 117 to 154 mm, and rainfall ranged from 83 to 126 mm. Monthly rainfall deficit ranged from −22 to −62 mm from May to October. A mix of positive and negative trends was observed at various temporal scales. An upward trend during January, April, June–November, winter, summer, autumn, and annual rainfall was observed, but only those trends in September and autumn were significant at a 95% confidence level. Rainfall increased by 0.35 mm each August and by 1.06 mm in autumn every year. Insignificant downward trends in rainfall in February, March, May, and December and in spring were detected. In contrast, decreasing trends were found for most months except February–April, all seasons, and annual ET_o. The significant downward trends in ET_o were observed in January, May–October, summer, and autumn. The decline in ET_o ranged from 0.05 to 0.29 mm each year. Only one significant increasing trend in DI of 0.054 was found in August, although all remaining months except April also exhibited upward trends. Autumn and annual trends in DI decreased by 0.006 and 0.001, respectively.

Monthly and annual ARIMA forecast models were fitted for prediction of rainfall, ET_o, and DI in the future. Low values of RRMSE (from −4.68 to 1.70), RMAE (from −3.67 to 1.30), PBIAS (from −0.11 to 0.91), and RSR (from 0.00 to 0.07) and high values of EF (1.0) and *D* (1.0) suggest that these models could be used

TABLE 8. As in Table 7, but for ET_o.

	Measured (mm)		Predicted (mm)							
	Mean	STDev	Mean	STDev	RRMSE	RMAE	EF	PBIAS	RSR	*D*
Jan	40.45	7.70	40.18	4.19	0.18	0.14	1.0	−0.01	0.006	1.0
Feb	49.30	9.54	47.48	4.60	0.17	0.14	1.0	−0.03	0.007	1.0
Mar	86.80	11.29	86.42	4.87	0.12	0.10	1.0	0.00	0.009	1.0
Apr	117.31	7.79	117.26	4.82	0.07	0.05	1.0	0.00	0.007	1.0
May	146.26	8.62	147.51	4.77	0.06	0.04	1.0	0.01	0.007	1.0
Jun	153.68	10.43	154.91	5.18	0.06	0.05	1.0	0.01	0.008	1.0
Jul	156.60	10.33	157.37	5.13	0.06	0.04	1.0	0.00	0.008	1.0
Aug	147.38	8.98	147.29	4.69	0.05	0.04	1.0	0.00	0.006	1.0
Sep	122.09	8.76	122.71	5.40	0.07	0.05	1.0	0.00	0.007	1.0
Oct	94.12	7.64	93.92	4.19	0.07	0.05	1.0	0.00	0.005	1.0
Nov	57.41	6.35	56.80	3.99	0.11	0.09	1.0	−0.01	0.005	1.0
Dec	38.85	6.88	38.21	3.48	0.17	0.13	1.0	−0.01	0.005	1.0

TABLE 9. As in Table 7, but for monthly logarithm of DI.

	Measured		Predicted							
	Mean	STDev	Mean	STDev	RRMSE	RMAE	EF	PBIAS	RSR	*D*
Jan	−1.05	0.60	−1.03	0.15	−0.57	−0.43	1.0	−0.01	0.0005	1.0
Feb	−0.87	0.55	−0.90	0.09	−0.64	−0.52	1.0	0.04	0.0004	1.0
Mar	−0.35	0.68	−0.36	0.08	−1.95	−1.43	1.0	0.02	0.0005	1.0
Apr	0.17	0.80	0.27	0.21	−4.68	−3.67	1.0	0.49	0.0006	1.0
May	0.58	0.76	0.64	0.19	1.31	1.02	1.0	0.07	0.0006	1.0
Jun	0.75	0.80	0.73	0.10	1.08	0.82	1.0	−0.02	0.0006	1.0
Jul	0.44	0.65	0.47	0.10	1.48	1.13	1.0	0.06	0.0005	1.0
Aug	0.75	0.87	0.79	0.12	1.17	0.90	1.0	0.05	0.0007	1.0
Sep	0.70	1.03	0.86	0.27	1.47	1.09	1.0	0.19	0.0008	1.0
Oct	0.64	1.10	0.80	0.27	1.70	1.30	1.0	0.21	0.0008	1.0
Nov	−0.33	0.75	−0.17	0.28	−2.24	−1.78	1.0	−0.40	0.0006	1.0
Dec	−1.03	0.66	−1.00	0.13	−0.65	−0.49	1.0	−0.02	0.0005	1.0

to predict monthly and annual rainfall, ET_o, and DI in the next 10 years. These models forecast 1319 mm of mean annual rainfall, 1203 mm of mean annual ET_o, and 0.082 of mean annual DI from 2015 to 2024.

This study presented a method to model and investigate monthly, seasonal, and annual distribution patterns, trends, and temporal variability in rainfall, ET_o, and water deficit to potentially improve water-management decisions in the local area that relies on data from this weather station. The purpose is to provide local professionals and producers who rely on data from this weather station with information on patterns and trends, a prediction tool for development of field water-management practices for greater water-use efficiency, and a demonstration of how to achieve such a goal at other locations using the same approach and method. For agricultural water management, the field researchers, extension specialists, farm consultants, and growers must often rely on a single nearby weather station to schedule irrigation and design cropping systems. Future work entails developing prediction tools and analyzing long-term data from other weather stations in the Blackland Prairie region to serve those professionals and producers who rely on other weather stations in the region and to investigate spatial patterns and variability of rainfall.

Acknowledgments. This project (62-2015) was funded by the Mississippi Soybean Promotion Board.

REFERENCES

Ahmed, K. F., G. Wang, and J. Silander, 2013: Statistical downscaling and bias correction of climate model outputs for climate change impact assessment in the U.S. Northeast. *Global Planet. Change*, **100**, 320–332, doi:10.1016/j.gloplacha.2012.11.003.

Ahuja, L. R., and L. Ma, 2002: Parameterization of agricultural system models: Current issues and techniques. *Agricultural System Models in Field Research and Technology Transfer*, L. R. Ahuja, L. Ma, and T. A. Howell, Eds., CRC Press, 273–316.

Akaike, H., 1974: A new look at the statistical model identification. *IEEE Trans. Autom. Control*, **19**, 716–723, doi:10.1109/TAC.1974.1100705.

Allen, R. G., L. S. Pereira, D. Raes, and M. Smith, 1998: Crop evapotranspiration—Guidelines for computing crop water requirements. U.N. Food and Agriculture Organization Irrigation and Drainage Paper 56, FAO, 300 pp. [Available online at http://www.fao.org/docrep/x0490e/x0490e00.htm.]

Arora, V. K., 2002: The use of the aridity index to assess climate change effect on annual runoff. *J. Hydrol.*, **265**, 164–177, doi:10.1016/S0022-1694(02)00101-4.

Birsan, M. V., P. Molnar, P. Burlamdo, and M. Pfaundler, 2005: Stream flow trends in Switzerland. *J. Hydrol.*, **314**, 312–329, doi:10.1016/j.jhydrol.2005.06.008.

Bronaugh, D., and A. Werner, 2013: Package 'zyp.' User guide for Zhang + Yue-Pilon trends package, 9 pp. [Available online at cran.r-project.org/web/packages/zyp/zyp.pdf.]

Budyko, M. I., 1974: *Climate and Life.* Academic Press, 507 pp.

Burn, D. H., and N. M. Hesch, 2007: Trends in evaporation for the Canadian prairies. *J. Hydrol.*, **336**, 61–73, doi:10.1016/j.jhydrol.2006.12.011.

Cleveland, W., 1979: Robust locally weighted regression and smoothing scatterplots. *J. Amer. Stat. Assoc.*, **74**, 829–836, doi:10.1080/01621459.1979.10481038.

Delitala, A., D. Cesari, P. Chesa, and M. Ward, 2000: Precipitation over Sardinia (Italy) during the 1946–1993 rainy season and associated large scale climate variation. *Int. J. Climatol.*, **20**, 519–541, doi:10.1002/(SICI)1097-0088(200004)20:5<519::AID-JOC486>3.0.CO;2-4.

Dyer, J., and A. Mercer, 2013: Assessment of spatial rainfall variability over the lower Mississippi River alluvial valley. *J. Hydrometeor.*, **14**, 1826–1843, doi:10.1175/JHM-D-12-0163.1.

Fisher, D. K., and H. C. Pringle III, 2013: Evaluation of alternative methods for estimating reference evapotranspiration. *Agric. Sci.*, **4**, 51–60, doi:10.4236/as.2013.48A008.

Gao, X., and F. Giorgi, 2008: Increased aridity in the Mediterranean region under greenhouse gas forcing estimated from high resolution simulations with a regional climate model. *Global Planet. Change*, **62**, 195–209, doi:10.1016/j.gloplacha.2008.02.002.

Hargreaves, G. H., and Z. A. Samani, 1982: Estimating potential evapotranspiration. *J. Irrig. Drain. Eng.*, **108**, 223–230.

Helsel, D. R., and R. M. Hirsch, 2002: Statistical methods in water resources. *Techniques of Water Resources Investigations*, chapter A3, Book 4, U.S. Geological Survey, 522 pp. [Available online at http://pubs.usgs.gov/twri/twri4a3/html/toc.html.]

Hobbins, M. T., J. A. Ramírez, and T. C. Brown, 2004: Trends in pan evaporation and actual evapotranspiration across the conterminous US: Paradoxical or complementary? *Geophys. Res. Lett.*, **31**, L13503, doi:10.1029/2004GL019846.

Hollinger, S. E., S. A. Isard, and M. R. Welford, 1993: A new soil moisture dryness index for predicting crop yields. *Eighth Conf. on Applied Climatology*, Anaheim, CA, Amer. Meteor. Soc., 187–190.

Karl, T. R., J. M. Melillo, and T. C. Peterson, 2009: *Global Climate Change Impacts in the United States.* Cambridge University Press, 188 pp.

Kendall, M. G., and J. D. Gibsons, 1990: *Rank Correlation Methods.* 5th ed. Oxford University Press, 260 pp.

Lázaro, R., F. S. Rodrigo, L. Gutiérrez, F. Domingo, and J. Puigdefábregas, 2001: Analysis of a 30-year rainfall record (1967–1997) in semi-arid SE Spain for implications on vegetation. *J. Arid Environ.*, **48**, 373–395, doi:10.1006/jare.2000.0755.

Legates, D. R., and G. J. McCabe, 1999: Evaluating the use of "goodness-of-fit" measures in hydrologic and hydroclimatic model validation. *Water Resour. Res.*, **35**, 233–241, doi:10.1029/1998WR900018.

Li, Z., F.-L. Zheng, and W.-Z. Liu, 2012: Spatiotemporal characteristics of reference evapotranspiration during 1961–2009 and its projected changes during 2011–2099 on the Loess Plateau of China. *Agric. For. Meteor.*, **154-155**, 147–155, doi:10.1016/j.agrformet.2011.10.019.

Liu, L., and Coauthors, 2012: Analyzing projected changes and trends of temperature and precipitation in the southern USA from 16 downscaled global climate models. *Theor. Appl. Climatol.*, **109**, 345–360, doi:10.1007/s00704-011-0567-9.

Liu, X., X. Mei, Y. Li, Q. Wang, J. Jensen, Y. Zhang, and J. Porter, 2009: Evaluation of temperature-based global solar radiation models in China. *Agric. For. Meteor.*, **149**, 1433–1446, doi:10.1016/j.agrformet.2009.03.012.

Lu, J., G. Sun, S. G. McNulty, and D. M. Amatya, 2005: A comparison of six potential evapotranspiration methods for regional use in the southeastern United States. *J. Amer. Water Resour. Assoc.*, **41**, 621–633. [Available online at http://www.srs.fs.usda.gov/pubs/ja/ja_lu004.pdf.]

Ma, L., and Coauthors, 2011: A protocol for parameterization and calibration of RZWQM2 in field research. *Methods of Introducing System Models into Agricultural Research*, L. Ahuja and L. Ma, Eds., Soil Science Society of America, 1–64.

——, T. J. Trout, L. R. Ahuja, W. C. Bausch, S. A. Saseendran, R. W. Malone, and D. C. Nielsen, 2012: Calibrating RZWQM2 model for maize responses to deficit irrigation. *Agric. Water Manage.*, **103**, 140–149, doi:10.1016/j.agwat.2011.11.005.

Makridakis, S., S. Wheelwright, and R. Hyndman, 1998: *Forecasting Methods and Application.* 3rd ed. John Wiley and Sons, 636 pp.

McKee, T. B., N. J. Doesken, and J. Kleist, 1993: The relationship of drought frequency and duration to time scales. *Eighth Conf. on Applied Climatology*, Anaheim, CA, Amer. Meteor. Soc., 17–22.

Mishra, A. K., and V. P. Singh, 2010: A review of drought concepts. *J. Hydrol.*, **391**, 202–216, doi:10.1016/j.jhydrol.2010.07.012.

Moriasi, D. N., J. G. Arnold, M. W. Van Liew, R. L. Gingner, R. D. Harmel, and T. L. Veith, 2007: Model evaluation guidelines for systematic quantification of accuracy in watershed simulation. *Trans. ASABE*, **50**, 885–900, doi:10.13031/2013.23153.

Nastos, P. T., N. Politi, and J. Kapsomenakis, 2013: Spatial and temporal variability of the aridity index in Greece. *Atmos. Res.*, **119**, 140–152, doi:10.1016/j.atmosres.2011.06.017.

Norrant, C., and A. Douguedroit, 2006: Monthly and daily precipitation trends in the Mediterranean (1950–2000). *Theor. Appl. Climatol.*, **83**, 89–106, doi:10.1007/s00704-005-0163-y.

Palmer, W. C., 1965: Meteorological drought. Weather Bureau Research Paper 45, 58 pp. [Available online at https://www.ncdc.noaa.gov/temp-and-precip/drought/docs/palmer.pdf.]

——, 1968: Keeping track of crop moisture conditions, nationwide: The new crop moisture index. *Weatherwise*, **21**, 156–161, doi:10.1080/00431672.1968.9932814.

Renard, B., and Coauthors, 2006: Evolution des extremes hydrométriques en France à partir de données observées (Observed changes in hydrological extremes in France). *Houille Blanche*, **6**, 48–54, doi:10.1051/lhb:2006100.

Roderick, M. L., M. T. Hobbins, and G. D. Earquhar, 2009a: Pan evaporation trends and the terrestrial water balance. II. Energy balance and interpretation. *Geogr. Compass*, **3**, 761–780, doi:10.1111/j.1749-8198.2008.00214.x.

——, ——, and G. D. Farquhar, 2009b: Pan evaporation trends and the terrestrial water balance. I. Principles and observations. *Geogr. Compass*, **3**, 746–760, doi:10.1111/j.1749-8198.2008.00213.x.

Sen, P. K., 1968: Estimates of the regression coefficient based on Kendall's tau. *J. Amer. Stat. Assoc.*, **63**, 1379–1389, doi:10.1080/01621459.1968.10480934.

Shumway, R., and D. Stoffer, 2011: *Time Series Analysis and Its Applications: With R Examples.* 3rd ed. Springer, 596 pp.

Turc, L., 1961: Evaluation des besoins en eau d'irrigation, evapotranspiration potentielle: Formule climatique simplifiée et mise a jour (Water requirements assessment of irrigation, potential evapotranspiration: Simplified and updated climatic formula). *Ann. Agron.*, **12**, 13–49.

Yoder, R. E., L. O. Odhiambo, and W. C. Wright, 2005: Evaluation of methods for estimating daily reference crop evapotranspiration at a site in the humid southeast United States. *Appl. Eng. Agric.*, **21**, 197–202, doi:10.13031/2013.18153.

Yürekli, K., H. Simsek, B. Cemek, and S. Karaman, 2007: Simulating climatic variables by using stochastic approach. *Build. Environ.*, **42**, 3493–3499, doi:10.1016/j.buildenv.2006.10.046.